Appl. Phys. B 38, 107–116 (1985)

Applied Physics B Photophysics and Laser Chemistry

Determination of the Nonlinear Optical Susceptibility $\chi^{(2)}$ of Surface Layers by Sum and Difference Frequency Generation in Reflection and Transmission

B. Dick, A. Gierulski, and G. Marowsky

Max-Planck-Institut für Biophysikalische Chemie, Abt. Laserphysik, Am Fassberg, D-3400 Göttingen, Fed. Rep. Germany

G. A. Reider

Technische Universität Wien, Institut für Allgemeine Elektrotechnik und Elektronik, Abteilung für Quantenelektronik und Lasertechnik, Gusshausstrasse 27–29, A-1040 Wien, Austria

Received 4 January 1985/Accepted 22 May 1985

Abstract. The theoretical investigation of sum and difference frequency generation in thin surface layers with rotational symmetry leads to formulas which connect the generated light intensities to the surface second order nonlinear susceptibility tensor. A maximum of seven tensor components can be determined in the case of lowest symmetry. Measurements in transmission should be especially useful since they allow easy variation of both polarization and angle of incidence. On the other hand, large signal enhancements are expected for total internal reflection geometries. A consistent set of $\chi^{(2)}$ tensor components for a thin layer of rhodamine-6G adsorbed on fused silica is found based on data from reflection and transmission measurements.

PACS: 42.65 Cq, 41

Already in the pioneer era of nonlinear optics it was recognized that nonlinear interaction of light waves in a medium with nonvanishing $\chi^{(2)}$ will lead to a reflected nonlinear beam in addition to the beam generated along the propagation direction of the fundamentals [1]. This was observed in second harmonic generation (SHG) by reflection from the surface of piezoelectric crystals [2, 3]. Lateron it was found that surfaces of centrosymmetric materials also can produce second harmonic light [4–7]. In the absence of any resonances of the material with the fundamental or harmonic light frequencies this effect can be explained by magnetic dipole [8] or electric quadrupole [5] contributions to $\chi^{(2)}$ as well as an electric dipole contribution from the first monolayer of material at the surface for which inversion symmetry is broken [9].

It was recognized by Shen [10–16] that the latter effect could be used to probe specifically adsorbed monolayers at surfaces employing an electronic resonance of the adsorbed molecules. The effect was demonstrated for several systems, e.g., rhodamine-6G at the fused silica/air interface [14], *p*-nitrobenzoic-acid at the interface of fused silica with air or ethanol [15] and silver electrodes covered with pyridine [13] and pyridazine [10]. It was shown that the shape of the resonance could identify the adsorbed molecules [14] and that polarized measurements could yield information about molecular orientation at the surface [14, 15]. Unlike other techniques using electron scattering (LEED) or photoelectron spectroscopy (UPS, XPS) for this purpose, this method is applicable to dense media and not restricted to UHV conditions.

All applications of the method so far involve generation of second harmonic by reflection from thin surface layers. The interpretation in terms of an orientational distribution is usually done by first assuming an orientational model allowing for only one degree of freedom. This means, a one-parameter

distribution function is assumed with the other orientational coordinate assumed either fixed [14] or random [15]. Within this model theoretical expressions for polarization ratios are calculated which, after comparison to the experimental result, give a value for the orientational parameter.

In this paper we extract a maximum of information about the surface properties without making any a priori assumptions about the orientational distribution. Rotational invariance around the surface normal (which can be checked quite easily) will result in seven independent tensor components of the surface second-order susceptibility $\chi^{(2)}$, which reduce to four in the case that the adsorbed molecules are non-chiral or a racemic mixture. In the case of degenerate photon energies only three tensor elements remain, which are the usual ones considered in surface second-harmonic generation.

Solution of Maxwell's equations leads to nonlinear waves at the sum and difference frequencies propagating in the directions of reflection and transmission. We will discuss both cases, since transmission is often more suitable for measurements of signal dependence from the angle of incidence. Furthermore, a nonlinear Brewster angle for which the component of the nonlinear beam polarized in the plane of incidence vanishes may exist in *reflection or transmission*. Finally, the choice of a special geometry can lead to total reflection of the signal beam accompanied by an enormous enhancement of signal strength.

The formulas presented should allow the determination of the surface tensor elements or at least their ratios from experiments done in reflection, transmission, and total reflection. These should lead to a consistent result for $\chi^{(2)}$ before any attempt of interpretation in terms of molecular orientation can be made. This theoretical method is applied to the analysis of SHG measurements on rhodamine-6G covered surfaces of fused silica in air.

1. Theory

1.1. Symmetry Considerations

Two light waves incident on a nonlinear medium will couple via the susceptibility $\chi^{(2)}$ to produce a polarization oscillating with the sum or difference of the ingoing light frequencies. In cartesian coordinates the relation between the amplitude vectors of the fields $E(1)$, $E(2)$, and the polarization P is

$$P_i^{\mathrm{NL}} = \sum_{jk} \chi_{ijk}^{(2)} E_j(1) E_k(2) . \tag{1}$$

Here $\chi^{(2)}$ is the macroscopic susceptibility of the sample, and the indices ijk refer to laboratory coordinates. For a system of noninteracting molecules $\chi^{(2)}$ is the ensemble average of the molecular susceptibility β:

$$\chi_{ijk}^{(2)} = \sum_{\mu\nu\varrho} \langle l_{i\mu} l_{j\nu} l_{k\varrho} \rangle \beta_{\mu\nu\varrho} . \tag{2}$$

The μ, ν, ϱ are coordinates defined in the molecular frame, the $l_{i\mu}$ are direction cosines, and the brackets indicate an average over a distribution function. If the components of β are known, the measurement of χ will yield information about the distribution function. Otherwise, if the distribution function is known, the molecular tensor β may be obtained. An example for the latter case are molecular crystals where the average is taken over all molecules in a unit cell.

Without a foreknowledge of the $\beta_{\mu\nu\varrho}$ the independent nonvanishing tensor components of χ can be found using symmetry properties of the distribution function. In this paper we consider the case of a surface which is invariant under rotation around the normal. Such distributions are expected on surfaces between amorphous, glassy, liquid, or gaseous phases. For the interface fused silica/air [14, 15] and fused silica/ethanol [15] the rotational invariance was found to hold.

The invariance condition for arbitrary rotations around the z-axis (defined as the surface normal) leaves only seven tensor components unrestricted

$$\begin{aligned}
&\chi_1 = \chi_{zzz} \\
&\chi_2 = \chi_{zxx} = \chi_{zyy} \\
&\chi_3 = \chi_{xzx} = \chi_{yzy} \\
&\chi_4 = \chi_{xxz} = \chi_{yyz} \\
&\chi_5 = \chi_{zxy} = -\chi_{zyx} \\
&\chi_6 = \chi_{xzy} = -\chi_{yzx} \\
&\chi_7 = \chi_{xyz} = -\chi_{yxz} .
\end{aligned} \tag{3}$$

And (1) takes the form

$$\begin{pmatrix} P_x \\ P_y \\ P_z \end{pmatrix}^{\mathrm{NL}} = \begin{pmatrix} 0 & 0 & 0 & \chi_7 & \chi_6 & \chi_3 & \chi_4 & 0 & 0 \\ 0 & 0 & 0 & \chi_4 & \chi_3 & -\chi_6 & -\chi_7 & 0 & 0 \\ \chi_2 & \chi_2 & \chi_1 & 0 & 0 & 0 & 0 & \chi_5 & -\chi_5 \end{pmatrix} \cdot \begin{pmatrix} E_x(1)E_x(2) \\ E_y(1)E_y(2) \\ E_z(1)E_z(2) \\ E_y(1)E_z(2) \\ E_z(1)E_y(2) \\ E_z(1)E_x(2) \\ E_x(1)E_z(2) \\ E_x(1)E_y(2) \\ E_y(1)E_x(2) \end{pmatrix} . \tag{4}$$

A mirror plane perpendicular to the surface as an additional symmetry element will cause χ_5, χ_6, and χ_7

to vanish

$$\chi^{(2)}=\begin{pmatrix}0&0&0&0&0&\chi_3&\chi_4&0&0\\0&0&0&\chi_4&\chi_3&0&0&0&0\\\chi_2&\chi_2&\chi_1&0&0&0&0&0&0\end{pmatrix}. \quad (5)$$

Such a mirror plane will always exist in a rotationally invariant distribution if the molecules forming the surface have mirror symmetry themselves or form a racemic mixture. The occurence of χ_5, χ_6, and χ_7 indicates chirality of the surface. (In a completely isotropic distribution of molecules only $\chi_5=-\chi_6=\chi_7$ can exist, e.g., in a solution of chiral molecules.) For the special case of second harmonic generation (SHG) the last three pairs of columns in (5) can be contracted:

$$\begin{pmatrix}P_x\\P_y\\P_z\end{pmatrix}^{\mathrm{NL}}=\begin{pmatrix}0&0&0&0&\chi_3&0\\0&0&0&\chi_3&0&0\\\chi_2&\chi_2&\chi_1&0&0&0\end{pmatrix}\cdot\begin{pmatrix}E_x^2\\E_y^2\\E_z^2\\2E_yE_z\\2E_xE_z\\2E_xE_y\end{pmatrix}. \quad (6)$$

This so called piezoelectric contraction is frequently used to write $\chi^{(2)}$ for SHG processes. All experimental work published so far on second order nonlinear optical effects at surfaces dealt with SHG only. We will use the full notation of (4), however, since we expect more data to be available in future from sum and difference frequency mixing experiments.

1.2. Generated Waves

The problem of the waves at the sum and difference frequencies radiated by the nonlinear polarization has been discussed in detail by Bloembergen and Pershan [1]. The appropriate model for the situation of interest is a thin parallel slab of nonlinear material between two linear media as shown schematically in Fig. 1. We will briefly review the definitions and results obtained with the method of [1].

In the general case two fundamental waves are refracted from the linear medium I into the nonlinear medium where they interact to form a nonlinear source wave

$$P^{\mathrm{NL}}=\chi^{(2)}:\varepsilon_1'\varepsilon_2'\cdot\exp[\mathrm{i}(k_1'+k_2')r-\mathrm{i}(\omega_1+\omega_2)t]=P^{\mathrm{NL}}\cdot\exp[\mathrm{i}(k_Sr-\omega_3t)]. \quad (7)$$

(ε' and k' refer to the fundamental beams in the nonlinear medium). In the case of SHG $k_S=2k_1'$ and

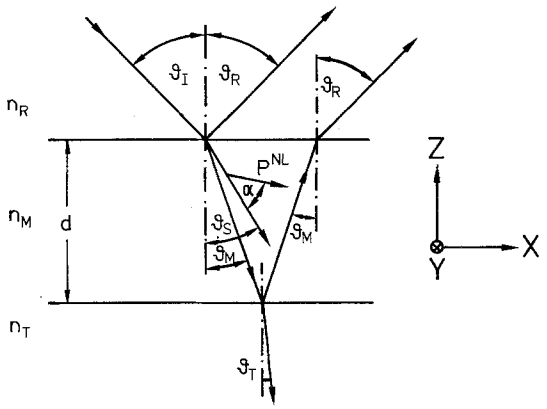

Fig. 1. Propagation of the nonlinear generated waves in a thin parallel slab. The fundamental waves are incident with angle ϑ_I and generate the nonlinear source wave propagating with angle ϑ_S. n_R, n_M, and n_T are the refractive indices for the generated waves, each written to the medium to which it applies. Four nonlinear waves are generated: one in reflection, one in transmission, and two propagating in the medium

the law of refraction requires $k_{1x}'=k_{1x}$ leading to

$$n_I\sin\vartheta_I=n_S\sin\vartheta_S, \quad (8)$$

where n_I and n_S are the refractive indices for the fundamental in the linear medium I and the nonlinear medium, respectively. A generalized n_S can be defined for sum and difference-frequency generation [1]. In the case of colinear propagation of the two fundamental beams in the nonlinear medium it is

$$n_S=(n_1'\omega_1+n_2'\omega_2)/(\omega_1+\omega_2), \quad (9)$$

where n_1' and n_2' are the refractive indices for the two fundamentals in the nonlinear medium. For our considerations it is only important to know that a nonlinear source wave characterized by n_S and ϑ_S is generated. The surface normal and k_S span the plane of incidence which we define as the xz-plane. The wavevectors of all generated waves will lie in this plane [1].

Maxwell's equations are solved for this system following the method outlined by Bloembergen and Pershan [1]. The continuity condition for the x and y components of the electric and the magnetic field at both interfaces imposes eight boundary conditions. As a consequence four nonlinear waves are generated (Fig. 1): One reflected (n_R, ϑ_R), one transmitted into the second linear medium (n_T, ϑ_T), and two propagating in the nonlinear medium (n_M, ϑ_M). The refractive indices n_R, n_T, and n_M refer to the generated frequency. The angles are related through the law of refraction by

$$n_T\sin\vartheta_T=n_R\sin\vartheta_R=n_M\sin\vartheta_M=n_S\sin\vartheta_S. \quad (10)$$

We assume that the active surface layer thickness d is much smaller than the wavelength of the generated

wave. In this case the phase shift of the waves between the two boundaries

$$\varphi_M = n_M \cos\vartheta_M d\omega_3/c \ll 1,$$
$$\varphi_S = n_S \cos\vartheta_S d\omega_3/c \ll 1, \tag{11}$$

are small and terms like $1-\exp(i\varphi_M)$ can be replaced by $-i\varphi_M$. The result for the reflected and transmitted waves are

$$\varepsilon_\perp^T = \varepsilon_\perp^R = \frac{4\pi i d\omega_3 P_\perp^{NL}/c}{n_R\cos\vartheta_R + n_T\cos\vartheta_T}, \tag{12}$$

$$\varepsilon_\parallel^R = -\frac{4\pi i d\omega_3 P_\parallel^{NL}/c}{n_T\cos\vartheta_R + n_R\cos\vartheta_T} \cdot\left[\cos\vartheta_T\sin(\vartheta_S+\alpha) + \frac{n_T}{n_M}\sin\vartheta_M\cos(\vartheta_S+\alpha)\right],$$

$$\varepsilon_\parallel^T = \frac{4\pi i d\omega_3 P_\parallel^{NL}/c}{n_T\cos\vartheta_R + n_R\cos\vartheta_T} \cdot\left[\cos\vartheta_R\sin(\vartheta_S+\alpha) - \frac{n_R}{n_M}\sin\vartheta_M\cos(\vartheta_S+\alpha)\right].$$

The indices $\parallel$ and $\perp$ denote the components of the generated radiation polarized parallel and perpendicular to the plane of incidence and α is the angle between k_S and P (Fig. 1). This result is identical with the one given by [1].

With a few algebraic manipulations we can eliminate α and contract the denominators yielding formulas in cartesian coordinates which can directly be connected to $\chi^{(2)}$

$$\varepsilon_\perp^T = \tilde{f}_y^T P_y^{NL}; \quad \varepsilon_\parallel^T = \tilde{f}_x^T P_x^{NL} + \tilde{f}_z^T P_z^{NL},$$
$$\varepsilon_\perp^R = \tilde{f}_y^R P_y^{NL}; \quad \varepsilon_\parallel^R = \tilde{f}_x^R P_x^{NL} + \tilde{f}_z^R P_z^{NL}, \tag{13}$$

with

$$\tilde{f}^R = \frac{4\pi i d\omega_3 \sin\vartheta_T}{cn_R\sin(\vartheta_R+\vartheta_T)} \cdot\begin{pmatrix} -\cos\vartheta_T/\cos(\vartheta_T-\vartheta_R) \\ 1 \\ (n_T/n_M)^2\sin\vartheta_T/\cos(\vartheta_T-\vartheta_R)\end{pmatrix}, \tag{14}$$

$$\tilde{f}^T = \frac{4\pi i d\omega_3 \sin\vartheta_T}{cn_R\sin(\vartheta_R+\vartheta_T)} \cdot\begin{pmatrix} \cos\vartheta_R/\cos(\vartheta_T-\vartheta_R) \\ 1 \\ (n_R/n_M)^2\sin\vartheta_R/\cos(\vartheta_T-\vartheta_R)\end{pmatrix}. \tag{15}$$

The factors $\tilde{f}$ can be regarded as nonlinear Fresnel factors describing the refraction of the nonlinear wave associated with P^{NL} into the media "R" and "T". The corresponding linear Fresnel formulas for the fundamental beams incident in the xz plane give the field ε' in

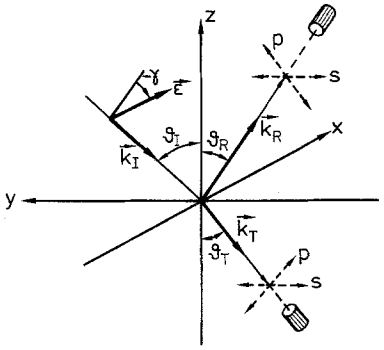

Fig. 2. Definition of experimental parameters. The plane of incidence is XZ, Z is the surface normal. The incoming beam has angle of incidence ϑ_I and angle of polarization γ with respect to the plane of incidence. The outgoing beams are generated in the direction ϑ_R (reflection) and ϑ_T (transmission) and analysed for their s and p polarized components

the nonlinear medium in terms of the incident field ε

$$\varepsilon_i' = f_i\varepsilon_i \quad i=x,y,z$$
$$f = \frac{2\sin\vartheta_U}{\sin(\vartheta_I+\vartheta_U)} \cdot\begin{pmatrix} \cos\vartheta_U/\cos(\vartheta_U-\vartheta_I) \\ \cos\vartheta_I \\ (n_I/n_U)\cos\vartheta_U/\cos(\vartheta_U-\vartheta_I)\end{pmatrix}, \tag{16}$$

where ϑ_I and ϑ_U are the angle of incidence and refraction for each beam related by

$$n_I\sin\vartheta_I = n_U\sin\vartheta_U. \tag{17}$$

In the case of SHG, $n_U = n_S$ and $\vartheta_U = \vartheta_S$. The same will be true when the two incident beams in sum frequency generation have at least approximately the same ratio n_I/n_U.

In an experiment we characterize the ingoing beams by their angle of incidence ϑ_I, angle of polarization with respect to the plane of incidence γ, and the intensity I. These are related with simple geometrical considerations to the cartesian components which are subsequently connected to $\chi^{(2)}$. For colinear incident beams and the tensor symmetry of (4) the result is (Fig. 2)

$$P_x^{NL} = \sqrt{I_1 I_2}\sin\vartheta_I[\cos\vartheta_I\cos\gamma_1\cos\gamma_2 \cdot(\chi_{xzx}f_{1z}f_{2x} + \chi_{xxz}f_{1x}f_{2z}) + \sin\gamma_1\cos\gamma_2\chi_{xyz}f_{1y}f_{2z} + \cos\gamma_1\sin\gamma_2\chi_{xzy}f_{1z}f_{2y}], \tag{18}$$

$$P_y^{NL} = \sqrt{I_1 I_2}\sin\vartheta_I \cdot[\sin\gamma_1\cos\gamma_2\chi_{xxz}f_{1y}f_{2z} + \sin\gamma_2\cos\gamma_1\chi_{xzx}f_{1z}f_{2y} - \cos\vartheta_I\cos\gamma_1\cos\gamma_2 \cdot(\chi_{xyz}f_{1x}f_{2z} + \chi_{xzy}f_{1z}f_{2x})], \tag{19}$$

$$P_z^{NL} = \sqrt{I_1 I_2}\,[\chi_{zxx}(f_{1x}f_{2x}\cos^2\vartheta_I\cos\gamma_1\cos\gamma_2 + f_{1y}f_{2y}\sin\gamma_1\sin\gamma_2) + \sin^2\vartheta_I\cos\gamma_1\cos\gamma_2\chi_{zzz}f_{1z}f_{2z} + \cos\vartheta_I\chi_{zxy}\cdot(f_{1x}f_{2y}\cos\gamma_1\sin\gamma_2 - f_{1y}f_{2x}\sin\gamma_1\cos\gamma_2)]\,. \quad (20)$$

In the case of SHG these reduce to

$$P_x^{NL} = I\cdot\sin\vartheta_I[\cos\vartheta_I\cos^2\gamma 2 f_x f_z\chi_{xxz} + 2\sin\gamma\cos\gamma f_z f_y\chi_{xyz}]\,, \quad (18a)$$

$$P_y^{NL} = I\cdot\sin\vartheta_I[2\sin\gamma\cos\gamma f_y f_z\chi_{xxz} - 2\cos\vartheta_I\cos^2\gamma f_x f_z\chi_{xyz}]\,, \quad (19a)$$

$$P_z^{NL} = I\cdot[\chi_{zxx}\cdot(f_x^2\cos^2\gamma\cos^2\vartheta_I + f_y^2\sin^2\gamma) + \chi_{zzz}f_z^2\cos^2\gamma\sin^2\vartheta_I]\,. \quad (20a)$$

The measured quantity is the intensity of the generated light polarized parallel (p) or perpendicular (s) to the plane of incidence:

$$I_s = |\tilde{f}_y P_y^{NL}|^2\,,\qquad I_p = |\tilde{f}_x P_x^{NL} + \tilde{f}_z P_z^{NL}|^2\,, \quad (21)$$

where the nonlinear Fresnel factors $\tilde{f}$ are taken from (14, 15) for reflection and transmission, respectively.

1.3. The Projection Model as Limiting Case

A simple projection model to describe surface second-harmonic generation is obtained when refraction at the boundaries to the surface layer is ignored and P^{NL} is calculated from χ and the cartesian components of the ingoing light fields. The field amplitudes ε_s and ε_p are found by projection of P^{NL} onto the appropriate polarization vectors. The result is

$$I_s \approx |P_y^{NL}|^2\,,\qquad I_p \approx |\cos\vartheta_R P_x^{NL} - \sin\vartheta_R P_z^{NL}|^2\,, \quad (22)$$

and the components of P^{NL} are given by (18–20) with all Fresnel factors set to unity.

Setting all refractive indices equal in the formulas of the preceeding section yields the same result, with the exception of an overall factor $(\cos\vartheta)^{-2}$. This factor causes divergence of the signal for horizontal incidence corresponding to infinite phase-matched propagation of the source wave and the second-harmonic wave through the nonlinear layer. Of course, the linear Fresnel factors will prevent such catastrophic behaviour.

Therefore, the projection model describes most of the qualitative features of the second-harmonic generation process well, whereas for quantitative evaluation all factors should be taken into account.

1.4. Nonlinear Brewster Angle

The intensity of the p-polarized signal is, according to (21), given by

$$I_p^R = \text{const}\cdot|\cos\vartheta_T P_x^{NL} - \sin\vartheta_T P_z^{NL}|^2\,,\qquad I_p^T = \text{const}\cdot|\cos\vartheta_R P_x^{NL} + \sin\vartheta_R P_z^{NL}|^2\,. \quad (23)$$

In case that P_x^{NL} and P_z^{NL} are of same order of magnitude an angle ϑ_T will exist for which I_p^R vanishes. If P_x^{NL} and P_z^{NL} have opposite sign and similar absolute magnitude, extinction of the signal will occur in transmission for a defined angle of incidence. Measurement of this Brewster angle [1] will directly give the ratio P_z/P_x which could be helpful in determining the relative sign of various components of the $\chi^{(2)}$ tensor. This latter effect has been used as null method by Heinz et al. [15].

1.5. Total Internal Reflection

In the case $n_R > n_T$ total reflection of the generated sum frequency beam can occur if the angle of incidence is chosen so as to make

$$\sin\vartheta_T = \frac{n_R}{n_T}\sin\vartheta_R = \frac{n_I}{n_T}\sin\vartheta_I > 1\,. \quad (24)$$

The situation is completely analogous to the linear case. As pointed out [1], all formulas remain valid with some of the trigonometric functions assuming complex values:

$$\sin\vartheta_T > 1\,,\quad \cos\vartheta_T = \mathrm{i}(\sin^2\vartheta_T - 1)^{1/2}\,,\quad \sin(\vartheta_T+\vartheta_R) = \sin\vartheta_T\cos\vartheta_R + \sin\vartheta_R\cos\vartheta_T\,,\quad \cos(\vartheta_T-\vartheta_R) = \cos\vartheta_T\cos\vartheta_R + \sin\vartheta_R\sin\vartheta_T\,. \quad (25)$$

Through $\cos\vartheta_T$ the z-component of k_T will become imaginary, and ε_T describes an evanescent wave.

However, in opposition to the linear case, where the sum of transmitted and reflected energy is always constant, in the case of nonlinear total reflection the signal can be considerably enhanced. This is exemplified in Fig. 3, where the SHG signal is simulated for a model surface with the fundamental approaching the surface from the side with lower refractive index (Fig. 3a) and higher refractive index (Fig. 3b), respectively. As soon as the angle of incidence reaches the critical value for total internal reflection the second-harmonic intensity increases about two orders of magnitude and becomes far larger than the combined intensities for transmitted and reflected SHG light for any angle of incidence in the other configuration of Fig. 3a. (note that the vertical scale is in the same units for both plots).

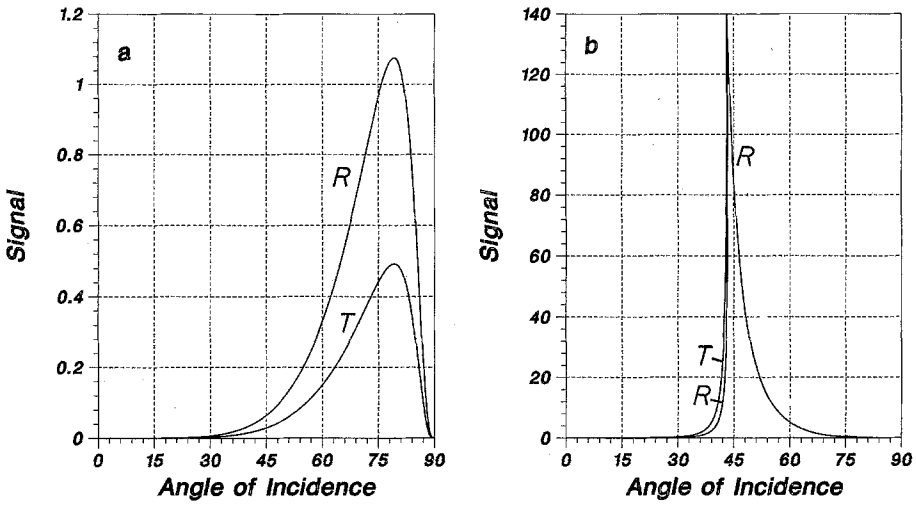

Fig. 3a and b. Simulation of SHG by surface reflection (R) and transmission (T) as a function of angle of incidence. (a) The fundamental beam approaches the boundary from the low index side (air). (b) The fundamental beam approaches the boundary from the high index side (fused silica). Note the strong enhancement of the signal as total internal reflection sets in

As a consequence of the total reflection the wave ε_p^R will exhibit a phase shift with respect to ε_s^R. When the ingoing waves are all linearly polarized this phase shift is given by

$$\eta = \arg(\varepsilon_p^R/\varepsilon_s^R) = \arg\left(\frac{\sin\vartheta_T P_z - \cos\vartheta_T P_x}{\cos(\vartheta_T - \vartheta_R) P_y}\right). \tag{26}$$

A phase shift of $\pi/2$ is found when

$$\frac{P_z}{P_x} = \frac{\cos\vartheta_R}{\sin\vartheta_R}\left(1 - \frac{n_T^2}{n_R^2 \sin^2\vartheta_R}\right). \tag{27}$$

This condition could be used to determine relative signs of tensor components of $\chi^{(2)}$ in a way similar to the Brewster angle condition.

1.6. The Problem of n_S and n_M

One major difficulty in using (14, 15) for quantitative evaluations of experiments is the question of choosing correct values for n_S and n_M, the refractive indices for the fundamentals and the sum or difference frequency in the surface layer. The refractive index n_M appears solely as a multiplicative factor in the nonlinear Fresnel factor $\tilde{f}_z$. The corresponding component of the polarization P_z contains χ_{zxx} and χ_{zzz}. Since these two tensor components do not appear in P_x and P_y, n_M assumes the role of a scaling factor for these two tensor components. Defining an effective $\chi^{(2)}$:

$$\chi_{\text{eff}}^{(2)} = (\chi_{zzz}/n_M^2,\ \chi_{zxx}/n_M^2,\ \chi_{xzx},\ \chi_{xxz}) \tag{28}$$

will eliminate n_M completely. This means, using (18–20) with n_M set to unity will give $\chi_{\text{eff}}^{(2)}$. No such simple contraction scheme exists to eliminate n_S and ϑ_S in the linear Fresnel factors. We are therefore left with the problem of finding n_S and – if we want to interprete $\chi^{(2)}$ in terms of an orientational model – also n_M.

The surface layers are too thin and the concentration of the dye molecules is too low to allow a direct measurement of the refractive indices by linear reflection studies [17]. However, n_S can be measured via the dependence of the nonlinear signal strength in transmission as a function of the angle of incidence. For s-polarized ingoing light and p-polarized detection the shape of this function does not depend on the magnitude of the susceptibility tensor elements

$$I_{\text{ssp}}(\vartheta) = \text{const} \cdot |f_y^2 \tilde{f}_z^T f'|^2, \tag{29}$$

where f' is the Fresnel factor for the refraction of the generated beam through the back surface of the glass substrate. The explicit form of (29) is

$$I_{\text{ssp}}(\vartheta) = \text{const} \cdot \frac{(\sin\vartheta_I)^{10}(\cos\vartheta_I)^4(\cos\vartheta_T)^2}{[\sin(\vartheta_S+\vartheta_I)\sin(\vartheta_R+\vartheta_T)\cos(\vartheta_R-\vartheta_T)]^4}. \tag{30}$$

Due to (10) n_S is the only unknown in (30). It is reasonable to assume that n_S is between the refractive indices for the fundamental in air and in silica glass. For $n_S = 1.01$ the maximum of I_{ssp} lies at $\vartheta_I = 82°$. [With $n_S = 1.0$ exactly, the curve $I_{\text{ssp}}(\vartheta)$ diverges for $\vartheta = 90°$ due to the $\cos^{-2}$ behaviour mentioned in Sect. 1.3.] With increasing n_S, i.e., with increasing glass character of the surface layer, the maximum shifts to smaller values of ϑ_I, reaching $\vartheta_{\max} = 62°$ when $n_S = n_{\text{glass}}$. A fit of (30) to the experimental curve will consequently yield a value for n_S. Taking $(n_S - 1)/(n_{\text{glass}} - 1)$ as the glass character of the surface layer, n_M can be estimated from n_T assuming that the glass character is frequency independent.

2. Experiment: Rhodamine 6G on Fused Silica

We apply the above given theory to the analysis of data obtained by second-harmonic generation from thin surface layers of rhodamine 6G on fused silica. This system was first studied by Shen and his coworkers

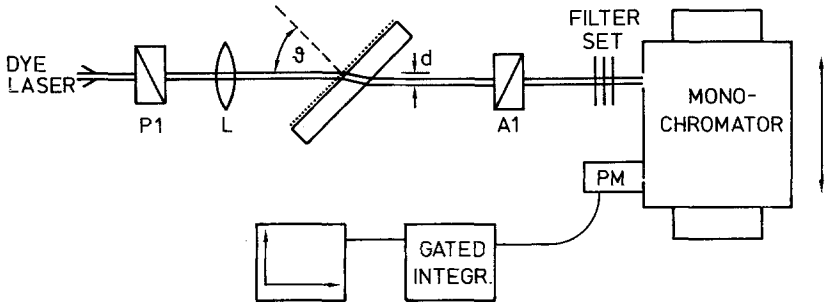

Fig. 4. Experimental arrangement for the determination of $I_{ssp}(\vartheta)$. The fused silica plate is rotated around the spot where the laser beam hits the surface with angle of incidence ϑ. A microprocessor controlled translation stage moves the detection system to compensate for the walkoff d of the second-harmonic beam

[14]. They proposed a surface model containing only one orientational parameter, namely the angle β between the molecular dipole axis and the surface normal. The molecular out-of-plane axis was restricted to lie in the surface plane. With the further assumption that β_{zxx} is the only nonvanishing molecular tensor element, and using the projection model with an angle of incidence of 45°, this leads to the prediction

$$\frac{I_{pp}}{I_{ss}} = \left(2\frac{\langle\cos\beta\rangle}{\langle\cos^3\beta\rangle} - \frac{3}{2}\right)^2, \tag{31}$$

where I_{pp} and I_{ss} are the second-harmonic intensities with the incident light polarized p and s, respectively. From a measurement of this polarization ratio the average orientation angle $\langle\beta\rangle$ can be obtained assuming that the distribution is sufficiently sharp to allow the substitutions

$$\langle\cos^n\beta\rangle =: \cos^n\langle\beta\rangle . \tag{32}$$

The restrictions of this model are obvious, and it is quite possible that the measured polarization ratio is the result of a completely different arrangement of the molecules in the surface layer. In fact, the model introduces the restriction

$$2\chi_{xxz} = -\chi_{zzz} \tag{33}$$

and a measurement of these macroscopic quantities could serve as a test. In our opinion all three independent tensor elements χ_{zzz}, χ_{zxx}, and $\chi_{xxz}=\chi_{xzx}$ should be determined before any assumptions about molecular tensor elements or orientation models are made.

Use of the projection model implicitely assumes $n_S = n_M = 1.0$, i.e., the surface layer is regarded as belonging to the medium air. Initially we believed this to be a reasonable guess, but measurement of the curve $I_{ssp}(\vartheta)$ according to (30) lead to a different conclusion. The experimental arrangement for this measurement is shown in Fig. 4. The axis of rotation of the glass substrate is carefully adjusted to lie exactly in the spot where the laser hits the surface. The beam walkoff d of the second-harmonic beam was compensated with a microprocessor controlled stepping motor system which moved the detection system synchroneously with the rotating fused silica plate in such a way that the second-harmonic beam always hit the photomultiplier at the same spot. This was important since the sensitivity of the photomultiplier tube varied considerably from spot to spot. The measured intensities as a function of the angle of incidence are shown in Fig. 5 (open circles). The full line shows the best fit to (30) obtained with the refractive index $n_S = 1.3286$. The values for n_S which lead to twice the sum of squares yield the confidence interval $n_S = 1.33 \pm 0.06$. The theoretical curve calculated with $n_S = 1.01$ and normalized to the same maximum is given as the dotted line. We are therefore forced to abandon the hypothesis of $n_S = n_{air}$ and rather have to assume an approximate 75% of glass character for the surface layer. Carrying this argument over to the second harmonic frequency we arrive at the values listed in Table 1 for the refractive indices appropriate to our experiments.

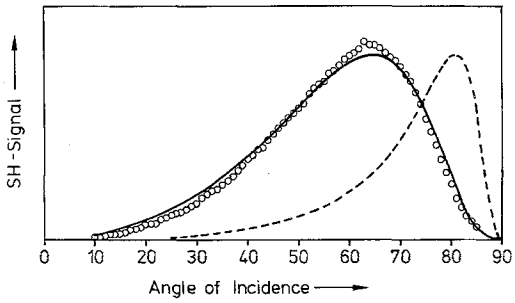

Fig. 5. Second harmonic signal strength as function of the angle of incidence in transmission through a fused silica window covered with rhodamine 6G. Open circles: experimental points. Full lines: best fit to (30) with $n_S = 1.3286$. Broken line: theoretical curve for $n_S = 1.01$. (For $n_S = 1.0$ the curve is dominated by the $\cos^{-2}$ artifact discussed in Sect. 1.3)

The three tensor components should be accessible through measurements of the s and p polarized signal intensities I_s and I_p for various angles of incidence ϑ_I and polarization γ. From (18–21) these are found to be

$$\begin{aligned} I_s &= |a_1 \sin(2\gamma)\chi_{xxz}|^2 , \\ I_p &= |\cos^2\gamma(a_2\chi_{xxz} + a_3\chi_{zxx} + a_4\chi_{zzz}) \\ &\quad + \sin^2\gamma a_5\chi_{zxx}|^2 . \end{aligned} \tag{34}$$

Table 1. Refractive indices of the glass plate and the surface layer for the fundamental beam (n, n_S) and the second harmonic beam (n_T, n_M). Values are given for the two fundamental wavelengths 660 and 695 nm used in our experiments

	660 nm	695 nm
n_1	1.4566	1.4550
n_S	1.3286	1.3276
n_T	1.4810	1.4775
n_M	1.3463	1.3438

The coefficients a_i are constant for a fixed angle of incidence

$$\begin{aligned} a_1 &= \sin\vartheta_I f_y f_z \tilde{f}_y, \\ a_2 &= \sin(2\vartheta_I) f_x f_z \tilde{f}_x, \\ a_3 &= \cos^2\vartheta_I f_x^2 \tilde{f}_z, \\ a_4 &= \sin^2\vartheta_I f_z^2 \tilde{f}_z, \\ a_5 &= f_y^2 \tilde{f}_z. \end{aligned} \tag{35}$$

We found it easiest to measure relative intensities for different polarizations keeping the angle of incidence fixed. Varying the angle of incidence always requires readjustment of the beams.
With the incident light polarized p ($\gamma=0$), s($\gamma=90°$) and intermediate ($\gamma=45°$) we obtain four intensities

$$\begin{aligned} I_1 &= I_s(45°) = |a_1 \chi_{xxz}|^2, \\ I_2 &= I_p(0°) \\ &= |a_2 \chi_{xxz} + a_3 \chi_{zxx} + a_4 \chi_{zzz}|^2, \\ I_3 &= I_p(90°) = |a_5 \chi_{zxx}|^2, \\ I_4 &= I_p(45°) \\ &= \tfrac{1}{4}|a_2 \chi_{xxz} + (a_3 + a_5)\chi_{zxx} + a_4 \chi_{zzz}|^2. \end{aligned} \tag{36}$$

Measurements of I_p alone cannot yield all three tensor elements since χ_{xxz} and χ_{zzz} always appear in the same linear combination. This leads to the relation

$$I_3 = (2\sqrt{I_4} - \sqrt{I_2})^2 \tag{37}$$

which was used to check the consistency of our data.
A straightforward analysis of the data could proceed via the following steps:
1) calculate the coefficients a_i for the particular choice of ϑ_I and refractive indices.
2) $\chi_{xxz} = \sqrt{I_1}/a_1$.
The sign is taken to be positive since the absolute sign is not accessible from intensity measurements.
3) $\chi_{zxx} = \pm\sqrt{I_3}/a_5$.
The sign of χ_{zxx} can be positive or negative with respect to χ_{xxz}.
4) $\chi_{zzz} = \dfrac{1}{a_4}(\pm\sqrt{I_2} - a_2\chi_{xxz} - a_3\chi_{zxx})$.
This will give four solutions for χ_{zzz} depending on the choice of sign for χ_{zxx} and $\sqrt{I_2}$.
5) Alternatively, I_4 leads to four different solutions:

$$\chi_{zzz} = \frac{1}{a_4}[\pm 2\sqrt{I_4} - a_2\chi_{xxz} - (a_3 + a_5)\chi_{zxx}].$$

6) The solution appearing in both sets is the correct result.
Although this method worked in principle, the results obtained for various angles of incidence did not agree well in the case of rhodamine 6G. The reason is that I_1 is small and the scatter of data is a considerable source of error for this intensity. Furthermore, the hierarchical structure of the analysis leads to accumulation of all errors in χ_{zzz}. A third problem is that the detection system has not strictly the same sensitivity for s and p polarized signals. We, therefore, developed a method of data analysis which:
i) equally distributes the error due to scatter of data,
ii) allows the inclusion of a larger number of data points obtained in different geometries and with different angles of incidence,
iii) does not require s polarized signal intensities.
For this purpose we define the following intensity ratios for a fixed angle of incidence:

$$\begin{aligned} \tilde{I}_1 &= I_1/I_3 = |\tilde{a}_1 \tilde{\chi}_{xxz}|^2, \\ \tilde{I}_2 &= I_2/I_3 = |\tilde{a}_2 \tilde{\chi}_{xxz} + \tilde{a}_3 + \tilde{a}_4 \tilde{\chi}_{zzz}|^2, \\ \tilde{I}_4 &= I_4/I_3 = \tfrac{1}{4}|\tilde{a}_2 \tilde{\chi}_{xxz} + \tilde{a}_3 + 1 + \tilde{a}_4 \tilde{\chi}_{zzz}|^2, \end{aligned} \tag{38}$$

where $\tilde{a}_i$ and $\tilde{\chi}$ are the appropriate quantities normalized to a_5 and χ_{zxx}. Labelling the intensities with a further index i counting experiments with different angle of incidence or geometry, the best choice for $\tilde{\chi}_{xxz}$ and $\tilde{\chi}_{zzz}$ is found by minimizing the quantity

$$S = \sum_{i=1}^{N} \sum_{k} (\tilde{I}_{ki}^{\text{calc}} - \tilde{I}_{ki}^{\text{exp}})^2. \tag{39}$$

Experimental intensities from six transmission and one reflection measurements were used for the fit. The minimum was found numerically with a Newton algorithm calculating derivatives via finite differences. Convergence is archieved within 5 to 7 cycles, and the result is the same for a large selection of starting points. The parameters a_i were calculated with the set of refractive indices in column 2 of Table 1 corresponding to the fundamental wavelength of 695 nm. The best fit is obtained with

$$\tilde{\chi}_{zzz} = 0.692; \quad \tilde{\chi}_{xxz} = -0.158. \tag{40}$$

The average rms deviation is 0.059 corresponding to 6% of the larger signals. Table 2 gives the experimental

Table 2. Intensity ratios $\tilde{I}_2$ and $\tilde{I}_4$ for several angles of incidence in reflection and transmission from fused silica covered with rhodamine 6G. The measured values are compared to the calculated ones for the best fit

Geometry	ϑ_I	Experimental		Calculated		
		$\tilde{I}_2$	$\tilde{I}_4$	$\tilde{I}_2$	$\tilde{I}_4$	$\tilde{I}_1$
T	30°	0.304	0.565	0.388	0.658	0.044
T	35°	0.338	0.615	0.411	0.674	0.043
T	40°	0.433	0.700	0.440	0.692	0.042
T	45°	0.483	0.717	0.474	0.713	0.041
T	50°	0.610	0.820	0.515	0.738	0.040
T	60°	0.640	0.860	0.628	0.803	0.036
R	45°	1.350	1.150	1.410	1.196	0.020

T: Transmission, R: Reflection

values I_i and the calculated values obtained with the best fit. The calculated values of $\tilde{I}_1$ show that these intensities should indeed be small. Experimentally they were found to be about one order of magnitude weaker than $\tilde{I}_4$. Figure 6 shows a simulation of $I_p(\vartheta, \gamma)$ for reflection and transmission with the parameters of the best fit. They predict that for the system rhodamine-6G on fused silica no Brewster angle situation exists.

To investigate the influence of the choice of refractive indices on the result of the fit, the procedure was repeated with several values for the refractive indices in the range $1.0 < n_S < 1.457$ and $1.0 < n_M < 1.481$ corresponding to the two linear media air and fused silica glass. In each case the optimization converged almost to the same sum of squares. Of course, the values found for $\tilde{\chi}_{zzz}$ and $\tilde{\chi}_{xxz}$ are different in each case. The ratio χ_{zzz}/χ_{xxz} is in the range between 3.3 and 4.5 and never agrees with (33). This suggests that the orientational model proposed by Heinz et al. [14] needs to be refined.

3. Conclusions

A method has been developed to determine the second-order nonlinear optical susceptibility tensor $\chi^{(2)}$ of a thin surface layer by sum or difference frequency generation experiments. It has been applied to the adsorbate system rhodamine 6G on fused silica in air. Data from second-harmonic generation obtained in reflection and transmission have been used in the analysis. The relative magnitude of the three independent tensor components χ_{zzz}, χ_{zxx}, and χ_{xxz} have been found by a least squares fit. Since the surface susceptibility is dominated by the resonant contributions of the adsorbed dye molecules, these relative tensor components can be compared to orientational models of the adsorbate system.

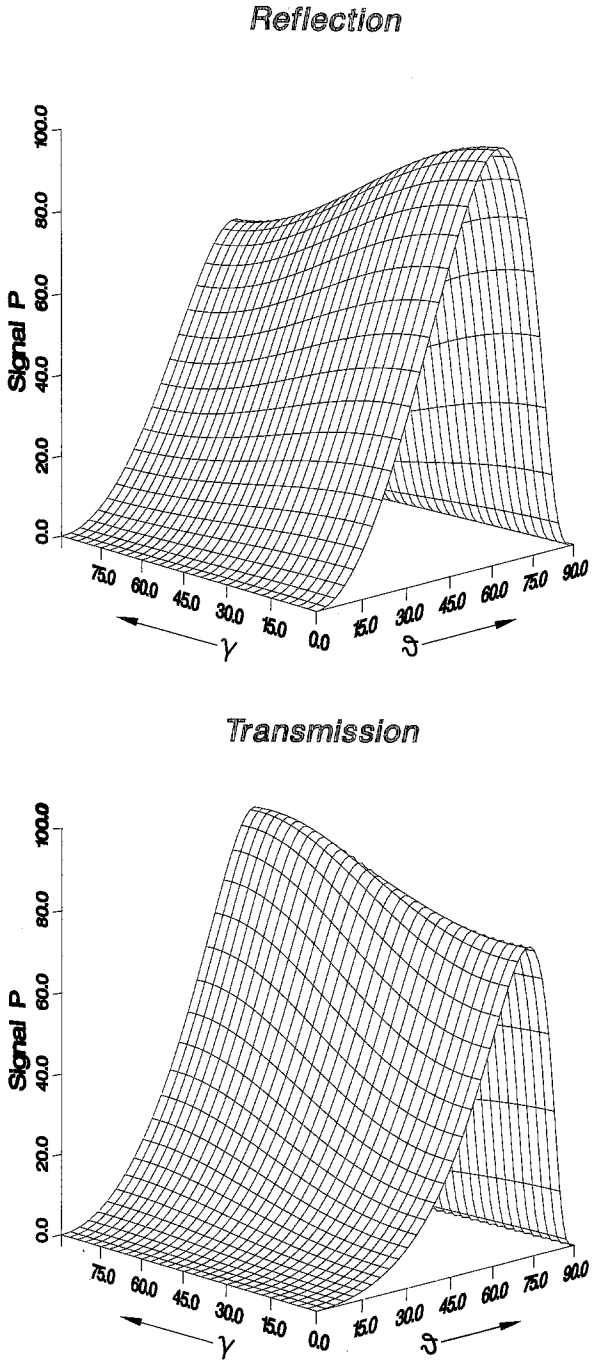

Fig. 6. Simulation of $I_p(\vartheta, \gamma)$ for reflection and transmission experiments. The parameters of the best fit have been used: $n_S = 1.3276$, $n_M = 1.3438$, $\chi_{zzz} = 0.692$, $\chi_{zxx} = 1.0$, $\chi_{xxz} = -0.158$

Acknowledgements. One of us (GAR) thanks the "Österreichischer Fond zur Förderung der wissenschaftlichen Forschung" for support under project No. P5273.

References

1. N. Bloembergen, P.S. Pershan: Phys. Rev. **128**, 606 (1962)
2. J. Ducuing, N. Bloembergen: Phys. Rev. Lett. **10**, 474 (1963)
3. R.K. Chang, N. Bloembergen: Phys. Rev. **144**, 775 (1966)
4. G.S. Agarwal, S.S. Jha: Solid State Commun. **41**, 499 (1982)
5. N. Bloembergen, R.K. Chang, C.H. Lee: Phys. Rev. Lett. **16**, 986 (1966)
6. C.H. Lee, R.K. Chang, N. Bloembergen: Phys. Rev. Lett. **18**, 167 (1967)
7. C.C. Wang, A.N. Duminski: Phys. Rev. Lett. **20**, 668 (1968)
8. F. Brown, R.E. Parks: Phys. Rev. Lett. **16**, 507 (1966)
9. F. Brown, M. Matsuoka: Phys. Rev. **185**, 985 (1969)
10. T.F. Heinz, C.K. Chen, D. Ricard, Y.R. Shen: Chem. Phys. Lett. **83**, 180 (1981)
11. C.K. Chen, T.F. Heinz, D. Ricard, Y.R. Shen: Chem. Phys. Lett. **83**, 455 (1981)
12. C.K. Chen, A.R.B. de Castro, Y.R. Shen: Phys. Rev. Lett. **46**, 145 (1981)
13. C.K. Chen, T.F. Heinz, D. Ricard, Y.R. Chen: Phys. Rev. Lett. **46**, 1010 (1981)
14. T.F. Heinz, C.K. Chen, D. Ricard, Y.R. Shen: Phys. Rev. Lett. **48**, 478 (1982)
15. T.F. Heinz, H.W.K. Tom, Y.R. Shen: Phys. Rev. A**28**, 1883 (1983)
16. C.K. Chen, T.F. Heinz, D. Ricard, Y.R. Shen: Phys. Rev. B**27**, 1965 (1983)
17. A. Penzkofer: Private communication